11TH INTERNATIONAL SYMPOSIUM ON PARTICLE IMAGE VELOCIMETRY – PIV15
Santa Barbara, California, September 14-16, 2015

DIC for Surface Motion Analysis Applied to Displacement of a Stent Graft for Abdominal Aortic Repair in a Pulsating Flow

Mikhail Tokarev[1], Håkan Roos[2], Håkan Nilsson[1] and Valery Chernoray[1]

[1] Department of Applied Mechanics, Chalmers University of Technology, Gothenburg, Sweden
tokarev@chalmers.se

[2] Department of Vascular Surgery, Sahlgrenska University Hospital, Gothenburg, Sweden

ABSTRACT

Stent graft migration has been recognized to influence the long-term durability of endovascular aortic repair. Flow-induced displacement forces acting on the attachment zones may contribute to this migration. An experimental perfusion model consisting of the flow loop described by Roos et al. [1] was used for further characterization of the pulsating flow induced stent graft movements with monocular and stereoscopic configurations of an optical imaging system. This paper adds new information on displacement measurement accuracy and 3D deformation analysis of the stent graft, which is used for abdominal aortic aneurysm treatment. The work describes used modification of Soloff's Stereo PIV reconstruction algorithm for surface motion analysis. It was found that the oscillation of the stent graft's body in the perpendicular direction to the front plane was 5 times less than side movements of the bent stent graft. These results can be used for further studies on different stent graft geometrical configurations and CFD simulations using fluid-structure interaction approach.

INTRODUCTION

Abdominal aortic aneurysm (AAA) has been reported to have increasing prevalence especially for older men**,** long-term smokers and those people who have high blood pressure in anamnesis. Endovascular aortic repair (EVAR) has been proved to reduce short-term morbidity and mortality during the treatment of the aortic aneurysms compared with open repair. However, EVAR has a higher risk of late complications and reinterventions [2, 3]. Many reinterventions are linked to migration of the stent graft and endoleaks of type I and III, related to insufficient seal at the stent graft attachments or interconnections respectively. Previous research [1, 4] has shown that the migration and endoleaks are linked with an insufficient anchoring of the stent graft. Stent grafts that are currently used for EVAR have hooks and barbs to prevent migration of the proximal (upstream) end of the stent graft. However, the distal (downstream) end does not have any additional mechanisms for fixation on the walls of the aorta except for the self-expanding force. As was previously reported by Resch et al. [4] the force needed to dislodge a stent graft with only self-expanding fixation is in the 2-4 N range. Biological incorporation has not been reported to provide any substantial support for stent graft fixation [4] because most migrations were diagnosed more than a year after an intervention. Roos et al. [1] found that the displacement forces have similar magnitude at both ends of the stent graft and that they increase with increased graft angulation and perfusion pressure but not with stroke frequency.

Several papers have presented results of computational studies for displacement forces. Li and Kleinstreuer [5] stated that the risk of a stent graft migration increases with its ratio between the inlet and outlet diameters. They also stated that the drag forces amplify with a higher aneurism neck angle, which is referred to as "angulation" in the current paper. Molony et al. [6] simulated the blood flow inside real abdominal aneurysm geometries of 10 post-operative AAA patients, obtained by CT scans. They concluded that the displacement forces correlated with perfusion pressure. Both studies used similar fluid-structure interaction simulations and reported that the contribution of the wall shear stress, or viscous component of the drag force, is negligible in comparison to the blood pressure or momentum change inside the stent graft. Three-dimensional MRI and CT scans of deployed real stent grafts after the EVAR were also analyzed by Figueroa et al. [7] with a following computer simulation inside the obtained geometry. CT scans by Waasdorp et al. [8] detected sideways movement of the stent graft. Sideways movement of the stent graft was also associated with an increased need for re-interventions.

Volodos et al. and Liffman et al. [9, 10] presented results of in vitro experiments measuring the displacement forces acting on the stent graft in pulsating flow conditions. Both experiments simulated an aneurysm sac with adjustable outer pressure. Volodos et al. [9] considered a straight graft geometry without angulation. The mean weight required to fix the PTFE graft with diameter 22 mm and atmospheric outside pressure was equal to 208.5 g. Liffman et al. [10] investigated dependence of the extraction forces needed to pull the modular stent graft apart inside an aneurysm sac on the pressure difference.

Measuring deformation and displacement of various objects is one of the most popular technique used in mechanical engineering in the design and testing of products and systems. And one of the most attractive methods of measurement is the photogrammetric approach, due to the nature of the non-contact measurement device design and the high degree of automation. The possibility of instantaneous measurements of a shape of an object opens very wide possibilities for the study of the processes of deformation and motion dynamics. There are currently a number of devices on the market for measuring shapes of bodies and their dynamics over time, for example Vic-3D from Correlated Solutions Inc. [11], StrainMaster from LaVision GmbH [12], etc. One of the directions of the European project AIM2, supervised by DLR, was dedicated to development of photogrammetric techniques for use in flight tests [13].

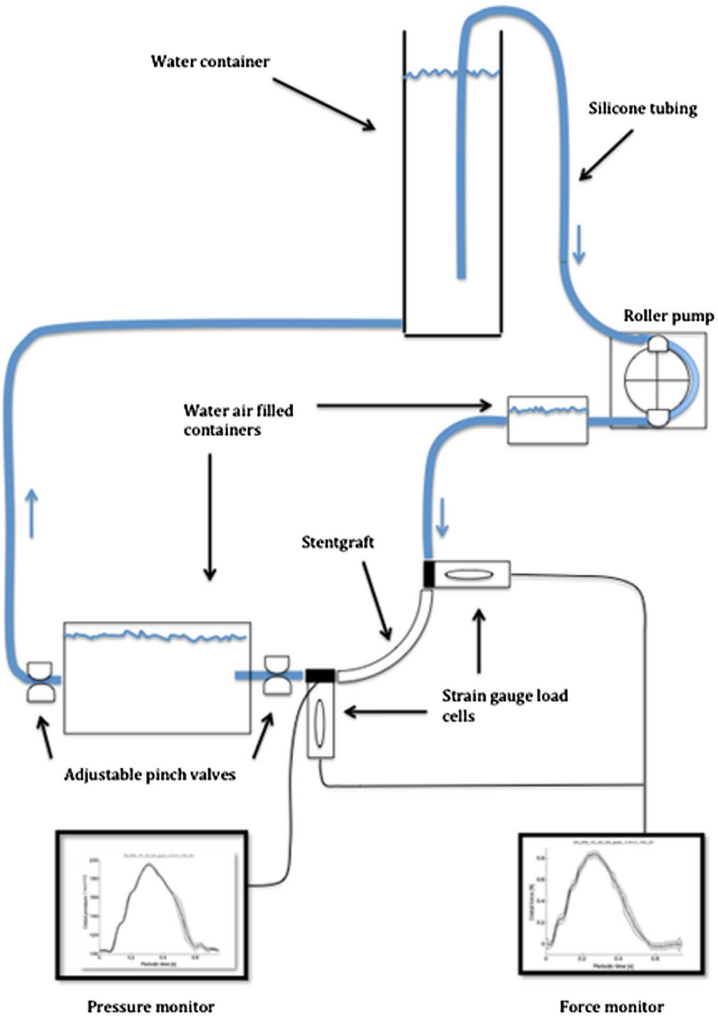

Figure 1 Scheme of the perfusion model

Among the used algorithmic implementations, one can distinguish the approaches of tracking a small number of selected markers on the surface of the object, correlation techniques (Digital Image Correlation/Image Pattern Correlation Technique), algorithms based on optical flow (Optical Flow), which have different capabilities for accuracy, spatial resolution, the requirements to the properties of the surface and its preparation. One of the possible directions of development of the method of photogrammetry is the use of the approaches developed for solving problems of

measurement of a velocity distribution in a fluid flow using movements of suspended particle-tracers in the flow volume (Stereo Particle Image Velocimetry, 3D Particle Tracking Velocimetry). A feature of these methods is the large number of points (particle-tracers) with the simultaneous measurement of velocity (tens of thousands or more), high precision measurements of displacements (0.1 pixel), the existence of procedures for error correction of calibration, the ability to measure with high temporal resolution (tens of kHz), etc. Much of the above is provided primarily by specialized image processing algorithms, allowing the basic configuration of measurement systems are simple enough to use.

The present work describes the usage of a standard PIV system for experimental fluid mechanics to measure the motion of the surface of a bent stent graft under pulsatile in vitro flow conditions. In addition, 3D displacement field measurements of the stent graft surface are provided to compare the displacement in the perpendicular direction with that obtained within the bend plane.

METHODS

An in vitro model of the pulsatile flow was used to establish a flow that was in the range of the expected physiological flow through an iliac limb stent graft. This perfusion model is shown in Figure 1. We used a digital image correlation technique to obtain displacements of the stent graft with pulsatile flow going through it. We measured 2D projections of the stent graft's surface displacement field in a direction perpendicular to the plane where the stent graft was located. For this purpose a digital camera was located perpendicular to the plane at the distance of 895 mm to it. It allowed us to analyze substantial side movements. Additionally, 3D displacements of its surface were measured using a stereoscopic optical setup in order to assess the value of normal to the plane dislocations of the stent graft. For the scheme of the optical measurement setup, please see Figure 2.

Photographs of the used cylindrical stent graft are shown in Figure 3. The stent graft is a complex device made of composite materials. It can be easily bent or compressed as it incorporates a metal serpentine spring. On the other hand, the stretching capabilities are quite limited because the rectified and unbent tube from Gore-Tex is less flexible than its supporting spring. However in our experiments the stent graft was slightly compressed, hence, for small deformations less than 2-3 millimeters it can be considered to a certain extent as a coil spring. As it can be seen from Figure 3 the serpentine spring frame has higher zig-zags in its middle position preventing the body from folding and following occlusion while being bent. Therefore the stent graft has inhomogeneous distribution of elasticity with more flexible parts closer to its ends. The curvature of the stent graft was evenly distributed along its length.

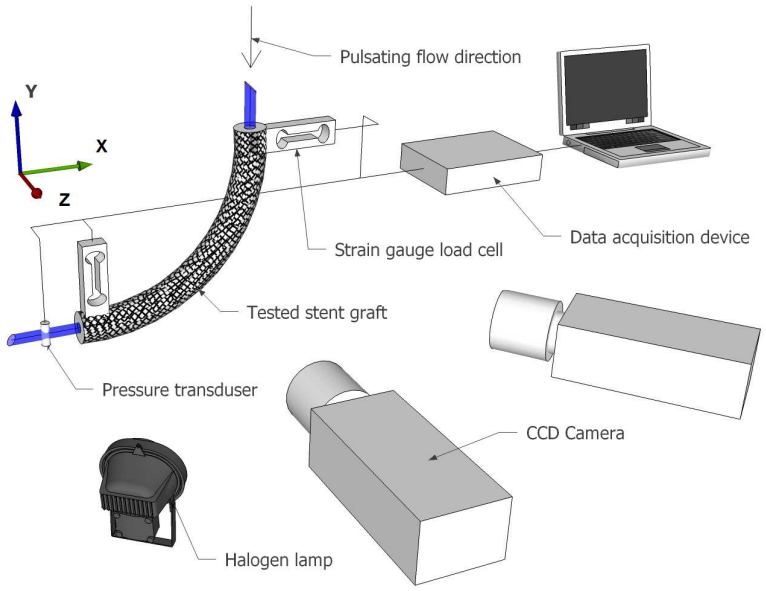

Figure 2 Scheme of an optical measurement setup

No special surface preparation of the stent graft was done. The original surface with the tube supported by a tubular nitinol serpentine spring was illuminated with a continuous light source. The registered images were masked to remove the background and were then used as an input for DIC analysis. According to preliminary tests the 2D correlation algorithm succeeded to determine the relative displacement between the unloaded and loaded stent graft using the original wired surface pattern shown in Figure 3. The opaque tube surface did not produce significant specular reflections because expanded PTFE (Teflon), from which the tubing was made, is a porous material with good scattering characteristics. The only problem with the stent graft tracking was water droplets leaking at the proximal attachment due to the insufficient seal of the proximal fitting. Sometimes moving refracting droplets led to displacement field's disturbances in that area.

We used a stereoscopic configuration for assessment of the third displacement component of the deformed arbitrary surface of the stent graft. This was done to ensure that the main dislocation occurred in the bending plane and that the normal to the plane displacement component can be neglected in our cases as well as contraction and expansion of the tubular graft. For this purpose we used a second camera observing the object on the right with the viewing angle 40 degrees to the plane and at the distance of 769 mm to it, see Figure 2. The camera position was extracted from its calibration parameters.

Both cameras were calibrated using a three-dimensional LaVision calibration object Type 11. For obtaining 3D surface deformation we analyzed stereoscopic images of the tested object before and after deformation. At first a depth map H(x, y) of the surface of the unloaded stent graft was calculated. The depth map was obtained by the standard method using disparity calculation of rectified stereo pairs through a local algorithm of optical flow calculation called a block-matching in the OpenCV library [16]. The depth map was then translated to the coordinate system defined by the calibrating object. For deformation calculation we used a modified algorithm for Stereo PIV reconstruction based on Soloff's approach [17]. Originally this method was proposed to calculate a three component displacement field in the laser sheet plane $z = 0$ for velocity measurements. During modification we substitute constant $z = 0$ by the surface depth $z=H(x, y)$ which was interpolated into the final regular grid (x_i,y_j). Displacement fields of the object upon the projections were obtained using a 2D PIV cross-correlation procedure. Thus for measurements of the 3D surface deformation we used two camera mappings, the unloaded object's depth map and two 2D deformation fields for the original images. The result is a 3D deformation field on a regular grid $(x_i, y_j, H(x_i, y_j), dx, dy, dz)$, where (dx, dy, dz) are those three components of the deformation field at the grid nodes (i, j).

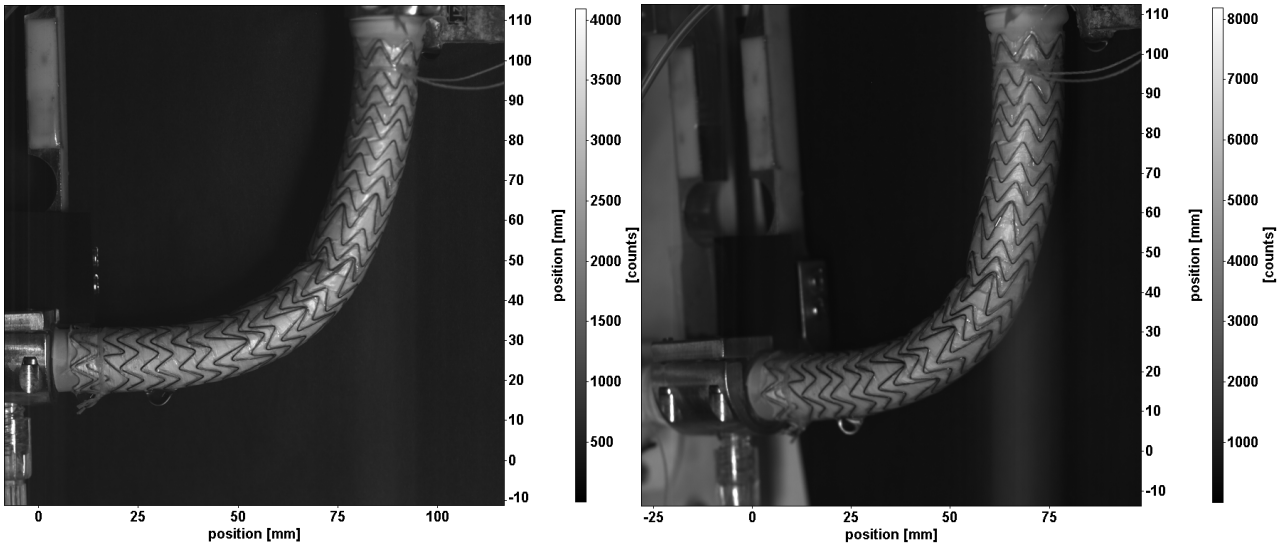

Figure 3 Photographs of two stereoscopic views of the anchored cylindrical stent graft with the fitting diameter 16 mm

We assessed the accuracy of the 3D deformation calculation algorithm described above using synthetic images of a deformed plate. The synthetic images were generated with the OpenGL functionality. This library allows users to create 3D graphics and has a required set of functions to create arbitrary texturing surface from finite elements in the form of triangles. The developed software simulated the deformation of an object surface and was able to use images of real surfaces as textures, which further enables us to obtain realistic input data for the measuring system with controlled deformation parameters.

The software used perspective projection with parameters *fovy* = 13 degrees and *aspect* = 1.78 (field of view angle and aspect ratio correspondingly) and near and far clipping planes at distances *z* = 3 and 5000 mm. A 3D model of a thin plate with sizes 120×48.5 mm was constructed by dividing into geometric primitives (a total of ≈50 000 elements), approximating a smooth surface. The plate model was textured with evenly distributed peak intensities of the Gaussian shape on the plane. The entire scene was filtered with the algorithm of anisotropic texture filtering to prevent blurring of the images of the plate at a considerable distance of the camera from the perpendicular to the plane of the plate.

The scene was projected onto three cameras located at points (0, 0, -300), ($\pm$300/($\sqrt{}$3), 0, -300) in mm. Optical axes of the virtual cameras intersected at the origin of coordinates. Thus, all the cameras were located at the distance 300 mm from the plane of the plate and the angle between adjacent cameras was 30 degrees. The pixel size of the cameras was equal 20 μm, wherein the focal length of the central camera was equal to 72mm.

A set of image projections with black circular markers 1.5 mm in diameter on a flat rectangular grid with the size 39×39 and distance 3 mm between neighboring markers was generated for camera calibration. The plane of the grid was sequentially located at the different depth distances z=0, 5, and 10 mm. The model images were saved with 8 bit quantization of the gray level in HD format (1920×1080 pixels). The error related to the noise in the images or the position of the calibration markers in the model was not simulated.

The deformation of the plate was performed by fixing its right edge (x=60mm) and moving its left edge (x=-60mm) perpendicular to the plane of the plate toward an observer. According to Sedov [14] a deformation of a thin plate takes on a parabolic profile, which was implemented in the framework of the model. The deformation was carried out with preservation of the original length of the plate (bending without stretching).

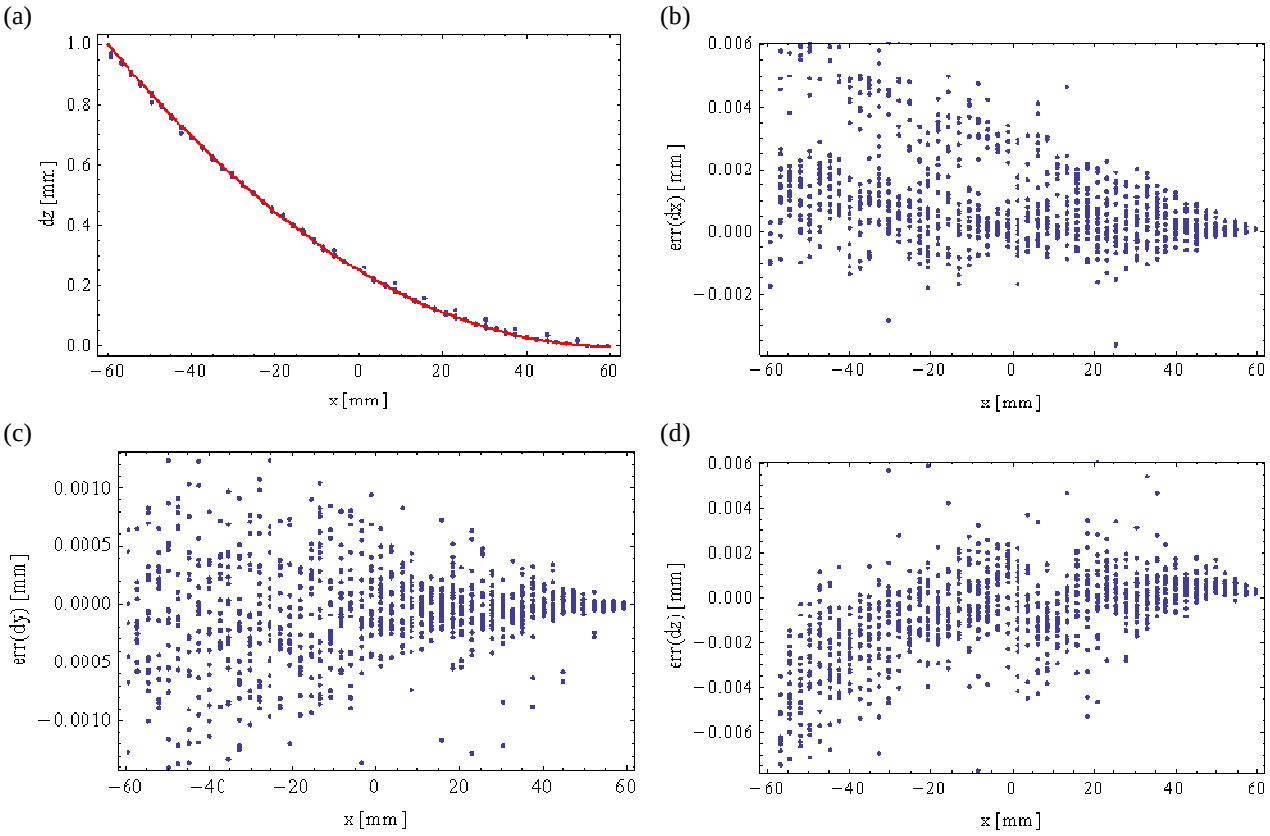

Figure 4 Results of the error analysis for the correlation algorithm using synthetic images. (a): Profile of the simulated plate deformation in a plane XZ with a 1 mm left side bend in the positive Z direction. Points show the calculated displacement component along the Z direction, and the solid line denotes a theoretical displacement profile. (b, c, d): The deviation of the calculated displacement components from the exact values for X, Y, and Z directions.

We compared the results of the correlation algorithm with results of an algorithm that can track the motion of individual points on a surface of a deformed body. This method triangulates densely located markers using its three registered projections. We applied the relaxation matching algorithm of the same markers on the original and deformed surfaces. This method was previously used by the authors to trace particles suspended in a volume of turbulent flow (3D PTV) [15]. Additionally we clustered markers that were located on a surface to remove outliers arising from ambiguity of correspondent points search during the triangulation process. The result of this algorithm is a field of three-dimensional deformation on an irregular grid in the form (x_k, y_k, z_k, dx_k, dy_k, dz_k), where k is an index of a tracked marker on a surface.

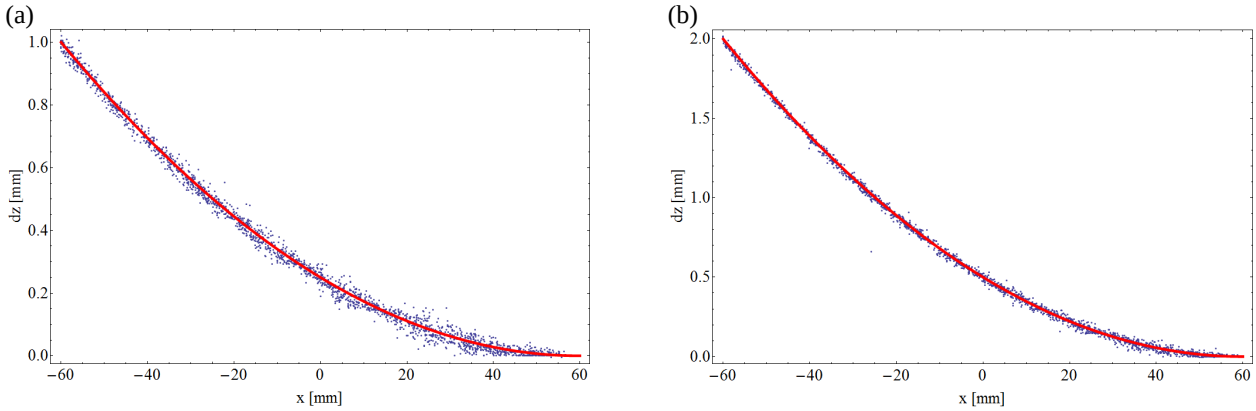

Figure 5 Profile of the simulated deformation of the plate in a plane XZ with (a) 1 and (b) 2 mm side bend toward positive Z direction. Points show the calculated deformation along Z direction. The solid line denotes a theoretical parabolic profile.

The results of an error assessment for the deformation measurements using the synthetic data of the thin plate bend are shown in Figure 4 and Figure 5. In this case, an element of a virtually infinite plate with coordinates x = -60mm was located at a distance z = 1 mm after bending. The left edge of x = -60mm (position without deformation) after deformation of the plate end was located 5 um closer to zero on the X axis compared to the unloaded state. The final grid during the calculation of the displacement using correlation analysis had the size of the cell equaled to 32 px. No cell overlapping was applied. The error was analyzed for 1089 measured points of the object.
It is seen that the best accuracy is achieved for measuring deformation along axis Y. For example, the 1 mm bend gave us the standard deviation 0.9 um (see Table 1), while the standard deviation of the measured deformations along the X and Z axes were near 6 um. This represents 0.6% of the amount of bending for the relative error.

Table 1 Assessment of deformation measurement accuracy using synthetic images of a deformed thin plate

	Correlation analysis			Surface points tracking		
Plate deformation dz(-60) cases [mm]	1	2	5	1	2	5
Bias error x, y, z [um]	1,6 -0,1 0,2	4,6 -0,08 0,9	17,2 0,02 2,6	-0,034 0,005 -3,4	-0,37 0,04 -4,2	-1,8 -0,07 -5,5
Random error x ,y, z [um]	6,4 0,9 5,9	11,8 1 7,3	19,5 1,8 15,6	26,9 4,6 17,5	61,7 4,7 19,3	121,7 4,6 24,7
Maximum absolute difference x, y, z [um]	104,5 12,8 79,7	145,8 12,3 50,8	91,3 20,8 20,5	943,4 10 85,2	1964,9 10 360,7	5196,7 10 616,8

For the analysis of individual markers during the triangulation the uncertainty area size was equaled to 4 px. Markers position identification was done by PMC (Particle Mask Correlation) method using particle template with the Gaussian intensity distribution variance 0.8. We used parameters of relaxation algorithms as follows: the maximum possible displacement – 1.5, 2.5, 5.5 mm (respectively for each case of 1, 2, and 5 mm bend), the radius of the current particle neighborhood - 10mm, maximum permitted value of displacement deviation 0.2, and the number of iterations is 3.

The random error of the deformation using the triangulation algorithm turned out to be 2 times higher than for the correlation algorithm and was about 20 um for the Z deformation component. Variation in the Y component also was significantly lower than the other components and was at 5 um. Variation in the X component increases with increasing of deformation, which may be caused by presence of outliers in the output of the relaxation algorithm. Due to the lower precision of the surface point tracking approach we have chosen the correlation approach for deformation measurements.

EXPERIMENTAL SETUP

For the measurements we used a 135 mm long Gore Excluder iliac limb stent graft (W. L. Gore & Associates, Inc., Newark, DE, USA) with 16 mm fitting diameter. A hydrodynamic loop with water was used to mimic in vivo aortic pressures and to establish a flow through the stent graft (see Figure 1). Three different perfusion pressures were investigated with fixed stroke rate at 60 b.p.m. An optical imaging system consisting of two synchronized cameras ImagerProX 4M (LaVision, Goettingen, Germany) with 2048 × 2048 pixel resolution with SIGMA AF 105 mm f/2.8 EX DG MACRO lens was used. Images were captured at 14.4 Hz, which made it possible to perform time-resolved object displacement measurements. Data processing was performed using the DaVis 8.2.2 software package (LaVision, Goettingen, Germany) for 2D correlation analysis, and in-house MATLAB and C++ codes for deformation fields post-processing and 3D deformation characterization. The stent graft movement was evaluated by image cross-correlation with images of the unloaded stent graft. The original tube surface supported by a tubular metal web was illuminated with halogen projectors of a total power 1.5 kW.

Two strain gauge load cells (Tadea-Huntleigh Model 1004; Vishay Transducers, Malvern, PA, USA) were installed to measure the forces at the ends of the stent graft. The relative measurement error for the strain gauge load cells was 0.0067%. We used a pressure transducer attached to the distal region of the stent graft to measure the pulse waveform, which was carefully adjusted to resemble in-vivo characteristics [1]. The type of pressure transducer was the Safedraw transducer blood sampling set (Argon Critical Care Systems, Singapore). A solar 8000 patient monitor (GE-Marquette, Milwaukee, WI, USA) was used to display the pressure curves.

The movements of the stent graft were captured close to the maximum available frame-rate of the digital cameras, with 14.4 Hz at full resolution and an exposure time of 250 us. This allowed us to get about 14 displacement fields per stroke and resolve the displacement fields referring to the aortic ejection event in time without synchronization with the stroke rate. It should be noted that although the stroke rate does not influence the extraction forces, a higher rate can lead to a faster migration of the stent graft due to the increased number of extraction acts for a certain period of time. The image data was registered for three different perfusion pressures 145/80, 170/90, and 195/100 mmHg, recording five times 100 images in order to have enough data for statistics of local extrema of displacements values.
We assessed the Reynolds number from the mean flow-rate Q taking into account the working principle of the two-roller peristaltic pump (HL-10; Gambro, Lund, Sweden), which squeezes one half of a circumference fluid volume of a flexible tube per stroke. The radius of the pump rotor was R = 70 mm, and internal diameters of the tubing and the stent graft were d = 12.7 mm and D = 16 mm correspondingly. Therefore the Reynolds number equaled to $\mathrm{Re} = \frac{QD}{\nu A} = \frac{\pi RSD}{\nu AT} = \frac{\pi Rd^2}{\nu TD} = 2217$, where A is the cross-sectional area of the stent graft, the stroke period T = 1 s as the stroke rate for all experiments was 60 b.p.m., and ν is the kinematic viscosity. This Reynolds number corresponded to the transitional flow regime in a pipe. While the mean flow-rate velocity through the stent graft with diameter D was 0.14m/s and flow-rate 1.7 L/min, the maximum velocity of the pulsating flow during a systolic phase is higher. Instantaneous velocity measurements inside the stent graft were not carried out at this time. This work focused mainly on integral parameters like the stent graft displacement and displacement forces caused by pulsating fluid motion.

DATA PROCESSING

The registered images were analyzed in the following way. At first we determined a spatial location of the maximum displacement within the unloaded graft's surface compared to the loaded state. Most of the time it was a position at the middle of the stent graft. For two-dimensional analysis of the displacement field an iterative correlation algorithm from the DaVis 8.2.2 software was utilized. The background area not related to the stent graft surface was masked with a manually selected rough polygonal area and a fine mask based on an intensity threshold value. The correlation analysis was performed with two passes by two iterations each. The first pass was done using 64 × 64 px interrogation area size and 50% overlap factor, while the second and final pass had 32 × 32 px areas with 25% overlap. We correlated a stationary image of

the stent graft without pulsating flow and those that were recorded during consecutive strokes. In order to avoid an outlier in determination of the maximum displacement location using only one time step we averaged the position of the maximum displacement location between first 100 time steps. Before averaging, the maximum location candidates were filtered out by a criterion that displacement direction must be in the fourth quadrant of the Cartesian plane within the range between 290 and 340 degrees. It was corresponded to the right down direction in Figure 6 (a), where the right direction coincides with x axis and the down direction is –y, as fluid inside the object was susceptible to a centrifugal inertial force during movement along a curved path down to the left. The point of maximum displacement is shown in Figure 6 (a) as Q, and a schematic representation of its x component displacement in time is shown in Figure 6 (b). It presents that in the unloaded condition when only static pressure was applied the point Q had the x coordinate value less than its mean value plus a half of the oscillation amplitude after enabling pulsating flow. Then a time history plot for a nearest neighboring point to the average maximum location was extracted. Finally, the end local maxima and minima were determined and its statistics was calculated for all the perfusion pressures. The displacement extrema in time were identified at the maximum displacement location point and at the lower and upper fixing points.

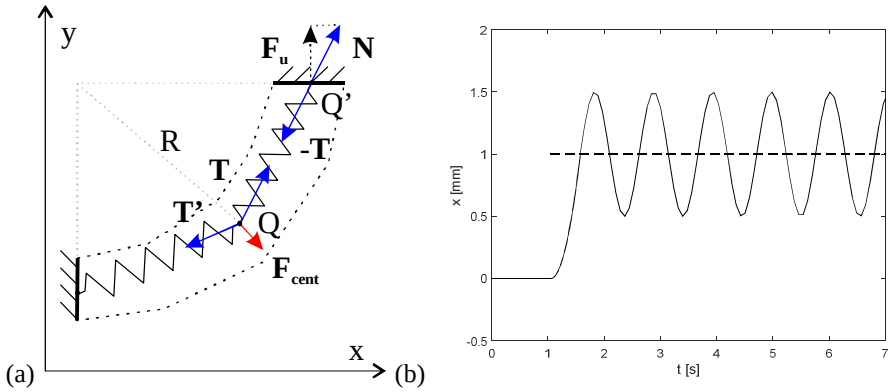

Figure 6 (a): Equivalent scheme of the flexible stent graft for 90 degrees symmetrical bend and distribution of forces (displacement force $\mathbf{F_{cent}}$ is marked with red color). (b) A schematic representation of a displacement oscillation for a point Q from the left graph before and after activation of the pulsating flow.

We will start by focusing on the fundamentals of movements of the bent cylindrical stent graft under a pulsating flow. It is illustrated in Figure 6 (a) in terms of a simplified equivalent scheme with two springs. Due to the momentum change of fluid inside the stent graft's bend an inertial (centrifugal) force $\mathbf{F_{cent}}$ occurs to prevent it. This force works against elastic forces **T** and **T'** of the stents graft's material, which increases with its deformation. The stent graft moves and deforms such that elastic forces equalize the inertial force. The higher the fluid velocity the more prominent displacement becomes. In this interpretation the upper strain gauge load cell measured projection $\mathbf{F_u}$ of the reaction force **N** in the direction of a flow. The similar situation is at the distal end. As it was stated by Roos et al. [1], both the proximal and distal ends undergo the same forces in magnitude. This occurs due to the symmetry of the current configuration, with an evenly distributed bend with curvature radius R. If the bend has a sudden drop of a curvature radius below R on one of its legs, for example when it has a fold, this will produce a displacement force redistribution between the two ends due to symmetry breaking.

RESULTS

Figure 7 and Figure 8 show examples of the 2D and 3D deformation results for the 90 degrees bent cylindrical stent graft with a maximal perfusion pressure 195/100 mmHg. The left images correspond to the deformation distribution, while the plots on the right refer to the time history of the point marked with the yellow circle in Figure 7 (a) characterized by maximal displacement values. The time history for the Z displacement in Figure 8 (b) looks noisier than that corresponding to the front plane displacement due to the smaller displacement oscillations in Z direction. According to the shown profiles, the maximum amplitude of displacement of the stent graft in this case is 0.24 mm, which is five time higher than it was in the out-of-plane direction. Therefore the stent graft movements can be analyzed only as 2D case.

Additionally, the accuracy of the surface 3D shape reconstruction was assessed as follows. The distance from the camera to a point of an object for a stereoscopic optical system is defined using the formula $Z = \frac{fT}{d}$, where f is a focal distance, T is a separation distance between cameras, and d is a disparity value in mm. Hence, the accuracy of the depth (surface shape)

measurements is expressed as $\Delta Z(Z) = \frac{Z^2}{fT}\Delta d$, where $\Delta d = \Delta px/16$ is the available resolution of the OpenCV algorithm for disparity calculation and Δpx is the a pixel size of the camera in mm [16]. Substituting real values in this expression we get the surface shape accuracy as $\Delta Z = 0.04$ mm or 40 um, which is of the same order as the displacement oscillation amplitude in the Z direction. This is the reason for the noise in Figure 8 (b). However, the mean deformation of the surface in the Z direction after enabling of the pulsating flow was identified with the satisfactory relative error of 13%.

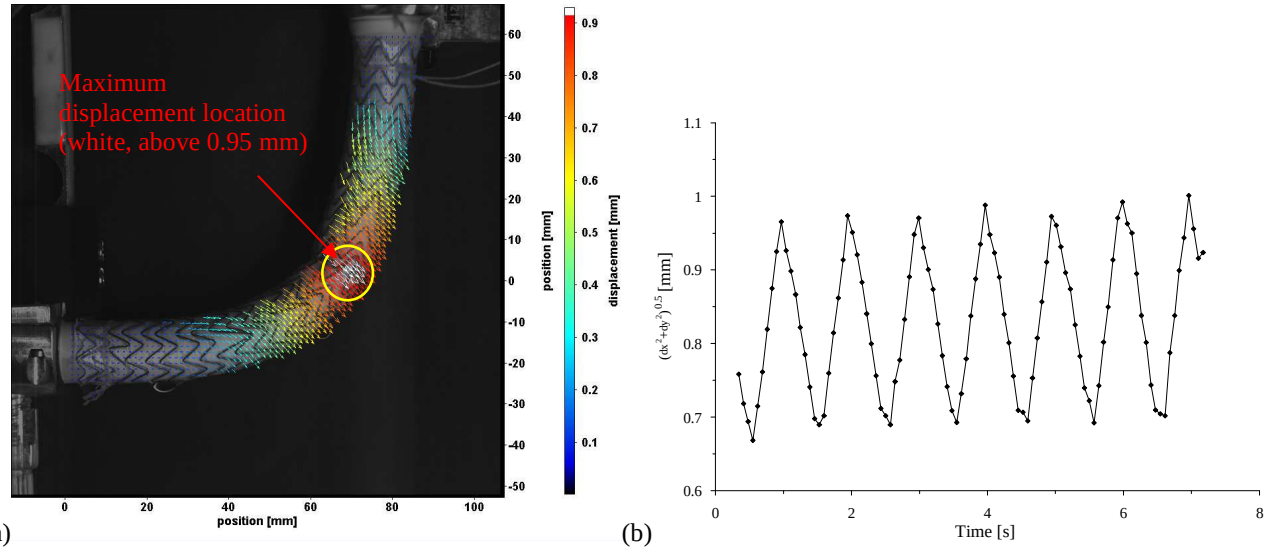

(a) (b)

Figure 7 Deformation of 90 degree bent stent graft with fitting diameter 16mm and perfusion pressure 195/100mmHg. (a): Photograph of the anchored stent graft with the estimated systolic 2D displacement magnitude field. (b): Time history of the stent graft displacement in a point with the maximum amplitude.

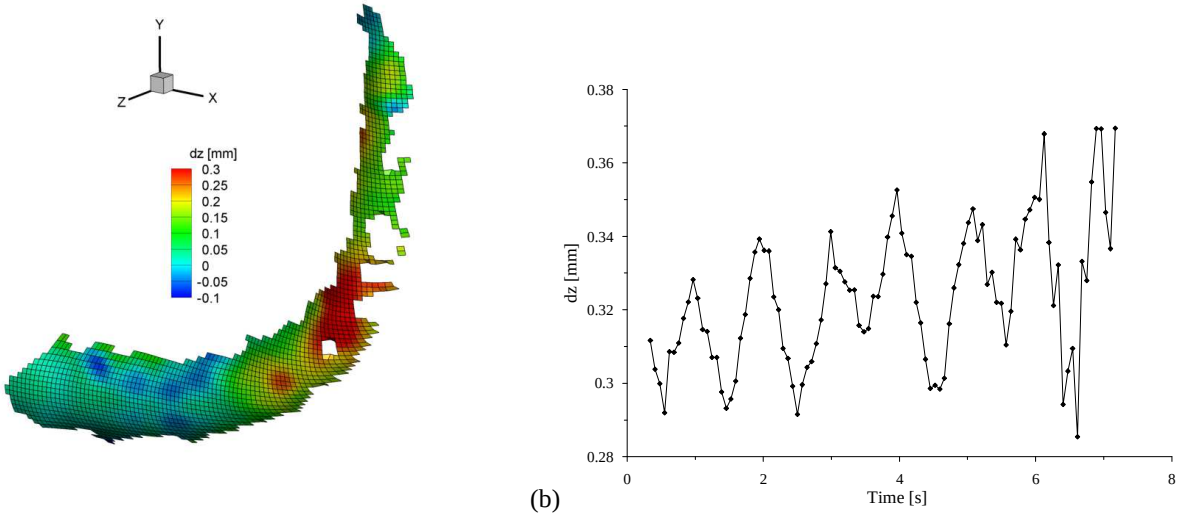

(a) (b)

Figure 8 Results of the measured displacements in Z direction for the 90 degrees bend with the fitting diameter 16 mm and perfusion pressure 195/100 mmHg. (a): Displacement of the stent graft surface in Z direction. (b): Time history of the stent graft displacement in a point with the maximum amplitude.

The error of the 2D deformation measurement was obtained using the DaVis 8.2.2 software and a-posteriory uncertainty quantification for PIV vector fields by correlation statistics [18], which is shown in Figure 9. Both bias and random errors are presented in this figure. The typical error values range from 2 um at the lower end and middle position up to 25 um at

the upper more shiny part of the stent graft. The error at the position of the maximum displacement was found to be about 10 um.

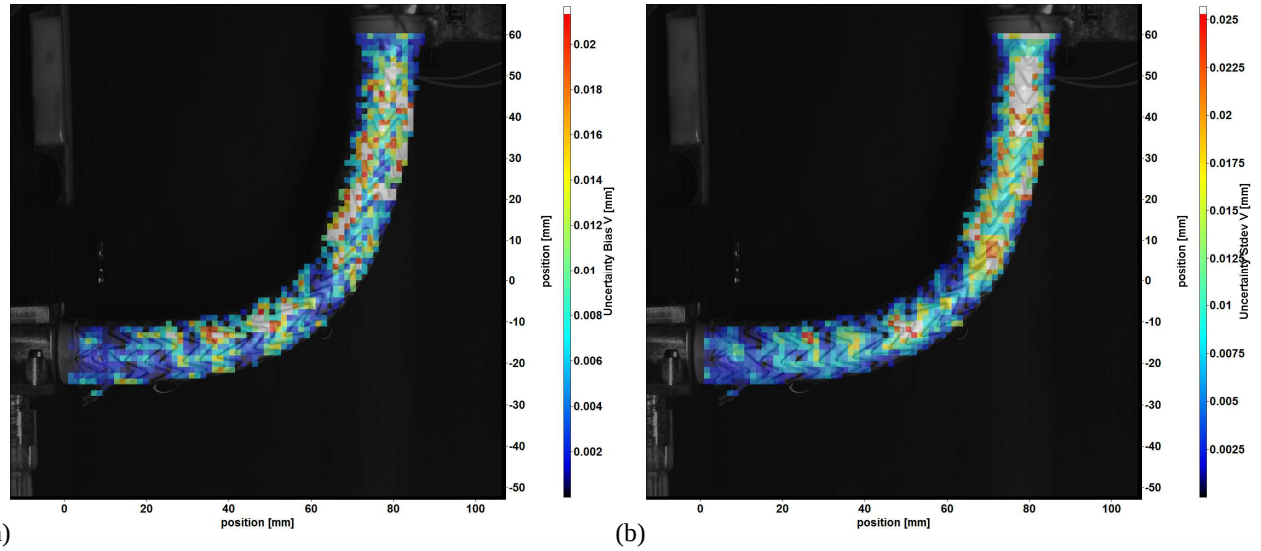

Figure 9 Results of error assessment for 2D correlation displacement calculations; (a): the bias error distribution, (b): the random error for different regions of the stent graft.

The final results of the measurements are summarized in Table 2. The table has two different parts, showing the maximum displacements within the stent graft and the displacements at the ends. The displacements are presented as a mean value around which the body of the stent graft was oscillated with some amplitude (after the slash) as it is depicted in Figure 6 (b). As the extrema max and min were obtained averaging several measurements these values are given the standard deviation in brackets. The X and Y maximum displacements are quite similar and increasing with the increase of the perfusion pressure. Here vertical displacements dominated in 10% compared to the horizontal ones. The maximum observed displacement magnitude was 0.95 mm (0.83+0.24/2).

Table 2 Summary of the obtained 2D displacements for different perfusion pressures

	Notation for displacements: (max+min)/2 (stddev) / max-min (stddev)		
Pressure [mmHg]	**145/80**	**170/90**	**195/100**
	Maximum displacements		
dx [mm]	0.38(0.005)/0.16(0.009)	0.46(0.008)/0.14(0.015)	0.55(0.007)/0.15(0.014)
-dy [mm]	0.41(0.004)/0.17(0.009)	0.52(0.006)/0.18(0.012)	0.62(0.009)/0.19(0.018)
$(dx^2+dy^2)^{0.5}$ [mm]	0.56(0.004)/0.24(0.008)	0.69(0.008)/0.23(0.009)	0.83(0.006)/0.24(0.012)
-dy/dx	**1.08**	**1.13**	**1.13**
	Displacements at the fixing points		
dx_l [mm] (Lower fix)	0.05(0.003)/0.05(0.005)	0.08(0.008)/0.04(0.016)	0.095(0.008)/0.042(0.016)
$-dy_u$ [mm] (Upper fix)	0.11(0.003)/0.07(0.007)	0.14(0.002)/0.07(0.005)	0.176(0.002)/0.076(0.005)
$-dy_u/dx_l$ (Upper/Lower)	**2.2**	**1.75**	**1.85**

If we consider movements in the fixing points they are close to the measurement error at the distal end for the lower pressure and reach up to 0.214 mm at the proximal end for the maximum pressure. It should be noted that displacements of the proximal end were near two times higher than at the distal end, which is linked with the less rigid upper strain gauge compared to the lower one, because the measurement range of the load cells was 0-2.8 N proximally and 0-5.6 N distally. It did not affect the force measurements since both load cells were properly calibrated. As for the extraction forces they were quite similar for both ends and increase with the pressure. All results are in agreement with Roos et al. [1]. The previously observed values of the displacements in the middle of the stent graft 0.22, 0.28, 0.29 mm for corresponding pressures were lower due to the manual selection of the tracking point and the higher tension of the stent graft between the two fixing points.

CONCLUSION

Measuring deformation and displacement of various objects is one of the most popular technique used in mechanical engineering in the design and testing of products and systems. And one of the most attractive methods of measurement is the photogrammetric approach, due to the nature of the non-contact measurement device design and the high degree of automation. In this paper a modification of the known Soloff's algorithm [17] for Stereo PIV data processing was applied for 3D surface motion reconstruction. Synthetic images of the deformed thin plate were used to assess the error for 3D deformation measurements by correlation and tracking techniques. The correlation method gave us 3 times less random error for the Z deformation component than separate points on a surface tracking approach in the case of small 1-2 mm deformations of the plate.

Results of an application of the surface motion analysis 2D and 3D in an experimental study of the displacements of the stent graft's body induced by a pulsating flow were presented. For this purpose an in vitro perfusion model that mimics a target part of the human circulatory system was used. The pressure pulse form was adjusted to be close to the real situation and the pressure outside the stent graft was atmospheric. Results were reported for mean displacement and oscillation amplitude at the location of the maximum displacement and at the fixation points of the 90 degrees bent cylindrical stent graft with the diameter 16 mm. In this study the detailed analysis of the measured displacement error was provided. The 2D measurement error was in the range from 2 um to 25 um within a deformation field.

Using stereoscopic imaging and digital image correlation (DIC) it was found that the stent graft's pulsating flow induced oscillations in the front plane were 5 times higher than in the out-of-plane direction, for example, 0.24 mm compared to 0.05 mm. For the currently used stereoscopic optical configuration and the stereo correspondence matching algorithm the surface depth estimation accuracy was found near 40 um. The relative error of the measured mean displacement in Z direction was 13%. According to the obtained results, the maximum mean displacement of the stent graft was 0.83 mm for the highest pressure with the mean displacement of the fixing points 0.095 mm and 0.176 mm for the distal and proximal end correspondingly.

ACKNOWLEDGEMENTS

The study was supported by the Gothenburg Medical Society (grant GLS-176311 and GLS-249441 to HR). Authors thank Leonid Kozinkin and Mikhail Karchevskiy for assistance with the synthetic images for the error analysis of the algorithms assessing 3D deformations.

REFERENCES

[1] Roos H, Ghaffari M, Falkenberg M, Chernoray V, Jeppsson, A, Nilsson H "Displacement forces in iliac landing zones and Stent graft interconnections in endovascular aortic repair: An experimental study" European Journal of Vascular and Endovascular Surgery 47 Issue 3 (2014) pp.262-267

[2] Greenhalgh RM, Brown LC, Powell JT, Thompson SG, Epstein D, Sculpher MJ "Endovascular versus open repair of abdominal aortic aneurysm." N Engl J Med 2010;362:1863-71.

[3] De Bruin JL, Baas AF, Buth J, Prinssen M, Verhoeven EL, Cuypers PW, et al. "Long-term outcome of open or endovascular repair of abdominal aortic aneurysm." N Engl J Med 2010;362: 1881-9.

[4] Resch T, Malina M, Lindblad B, Malina J, Brunkwall J, Ivancev K "The impact of stent design on proximal stent-graft fixation in the abdominal aorta: an experimental study." Eur J Vasc Endovasc Surg 20 (2000) pp.190-5.

[5] Li Z, Kleinstreuer C "Analysis of biomechanical factors affecting stent-graft migration in an abdominal aortic aneurysm model." J Biomech 2006;39:2264-73.

[6] Molony DS, Kavanagh EG, Madhavan P, Walsh MT, McGloughlin TM "A computational study of the magnitude and direction of migration forces in patient-specific abdominal aortic aneurysm stent-grafts." Eur J Vasc Endovasc Surg 2010;40:332-9.

[7] Figueroa CA, Taylor CA, Yeh V, Chiou AJ, Zarins CK "Effect of curvature on displacement forces acting on aortic endografts: a 3-dimensional computational analysis." J Endovasc Ther 2009;16: 284-94.

[8] Waasdorp EJ, Gorrepati ML, Rafii BY, de Vries JP, Zarins CK "Sideways displacement of the endograft within the aneurysm sac is associated with late adverse events after endovascular aneurysm repair." J Vasc Surg 2012;55:947-55.

[9] Volodos SM, Sayers RD, Gostelow JP, Sir Bell PR “An investigation into the cause of distal endoleaks: role of displacement force on the distal end of a stent-graft.” J Endovasc Ther 2005;12:115-20.

[10] Liffman K, Sutalo ID, Lawrence-Brown MM, Semmens JB, Aldham B “Movement and dislocation of modular stent-grafts due to pulsatile flow and the pressure difference between the stent graft and the aneurysm sac.” J Endovasc Ther 2006;13:51-61.

[11] http://www.correlatedsolutions.com/vic-3d/

[12] http://www.lavision.de/en/products/strainmaster/strainmaster-dic.php

[13] http://aim2.dlr.de/measurement-techniques/index.html

[14] Sedov LI “Continuum Mechanics. Volume 2” - M .: Nauka, 1970. - 568 p.

[15] Akhmetbekov YK, Lozhkin VA, Markovich DM, Tokarev MP “Multiset Triangulation 3D PTV and its Performance Compared to Tomographic PIV” Proc. 9th International Symposium on Particle Image Velocimetry., 21-23 July, Kobe, Japan, 2011.

[16] Bradsky G, Kaehler A “Learning OpenCV.”, O'Reilly, 2008

[17] Soloff SM, Adrian RJ, Liu Z-C “Distortion compensation for generalized stereoscopic particle image velocimetry”, Meas. Sci. Technol. 8 (1997) pp.1441-54

[18] Wieneke B “Generic a-posteriori uncertainty quantification for PIV vector fields by correlation statistics.” 17th Int Symp Appl Laser Tech Fluid Mech, Lisbon, Portugal, 2014.